RSC Advances

ROYAL SOCIETY OF CHEMISTRY

www.rsc.org/advances

An efficient gold nanocarrier for combined chemo-photodynamic therapy on tumor

Hongmei Li [a], Zhen Li [a], Lixiang Liu [a], Tao Lu [a] and Yue Wang* [a,b]

a School of Sciences, State Key Laboratory of Natural Medicines, China Pharmaceutical University, Nanjing 211198, China.

b Key Laboratory of Biomedical Functional Materials, China Pharmaceutical University, Nanjing 211198, China.

*Corresponding author: E-mail: zwy_1115@126.com

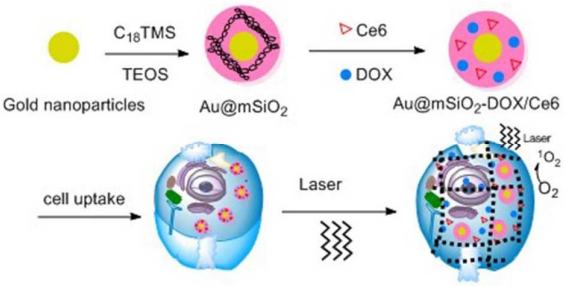

A multimodal Au@mSiO$_2$ nanocarrier in which AuNPs as PDT-assistor cores and mesoporous silica shells as supporters to load two drugs.

Cite this: DOI: 10.1039/c0xx00000x

www.rsc.org/xxxxxx

ARTICLE TYPE

An efficient gold nanocarrier for combined chemo-photodynamic therapy on tumour cells

Hongmei Li [a], Zhen Li [a], Lixiang Liu [a], Tao Lu [a] and Yue Wang*[a, b]

Received (in XXX, XXX) Xth XXXXXXXXX 20XX, Accepted Xth XXXXXXXXX 20XX

DOI: 10.1039/b000000x

A multimodal nanocarrier based on mesoporous silica coated gold nanoparticles (Au@mSiO_2) is developed for effective cancer treatment in vitro. Through introducing octadecyltrimethoxysilane (C_{18}TMS) as a porogen, the porosity of silica shells can be well controlled. The mesoporous silica offers high loading capacity for photosensitizer chlorin e6 (Ce6), thus improving the efficacy of singlet oxygen generation after the cellular uptake to achieve photodynamic therapy. Besides, Au@mSiO_2 with high surface area can also be used as a chemotherapy drug carrier to load Doxorubicin (DOX). Hence, Au@mSiO_2 nanocarrier combines photodynamic- and chemo-therapy together through simultaneously loading different types of therapeutic agents: Ce6 and DOX, which shows obviously synergistic cancer cell killing effect. Therefore, this Au@mSiO_2 nanocarrier would exhibit inspiring potential for cancer combination therapy.

Introduction

The application of nanomaterials in drug delivery has gained much attention in recent years and has become an important field in pharmaceutical research. Due to their large surface area, effective cellular uptake and controlled drug release, nanomaterials are emerging as appealing hosts of drug carriers [1-3]. However, diseases such as tumors, with dynamic changes in the genome and composed aberrant pathway network regulation, the actual effect and potential use of these drug carriers has been challenged[4, 5]. Combined different mechanisms of tumor therapies like chemotherapy and photodynamic therapy (PDT) using drug carriers have been proven highly effective for their ability to impact multiple disease pathways[6-8].

PDT, a selectively invasive technique for cancer therapy [9, 10], utilizes photosensitizer (PS[11]) and oxygen in tissues to induce reactive oxygen species (ROS) [12] under the light irradiation. ROS, such as singlet oxygen ($^1O_2$), which is cytotoxic and capable of killing cells nearby. PDT involves two vital procedures: firstly, PS is accumulated at the target organism, and then activated to generate $^1O_2$ for effective local therapy. However, the poor-water solubility of most PSs results in the failure to acquire an appropriate formulation to transport PS into the cell [13]. Besides, lack of proper selectivity to the tumor cells may produce severe side effects [14]. To solve these problems, alternative approaches of using nanocarriers to delivery porphyrin and its derivatives such as chlorin e6 (Ce6) have been studied by many research groups [15-18]. These nanocarriers are designed for localized drug delivery therapy aiming at increasing the accumulation of photosensitizer in the tumor to overcome the insolubility of the free photosensitizer thus alleviating the toxicity [19, 20].

Generally, individual nanoparticles (NPs) such as iron oxide, carbon nanotube, gold nanorods (GN), gold nanoparticles (Au NPs) and graphene oxide[21-24] are used to load PS on their surface in order to improve the uptake of PS by cells and then achieve PDT. Specially, GN and Au NPs have been broadly explored for drug delivery and PDT due to their strong light absorption at tunable plasmon resonance wavelength and facility to functional modification [25-27]. Au NPs with good biocompatibility and low toxicity set the stage for an ideal drug delivery system. In addition to their prominent safety, Au NPs could also act as both an ROS enhancer and a PS carrier. More interestingly, the highly localized plasmonic field of Au NPs can enhance generation of $^1O_2$ from PS thus may remarkably improve the PDT efficiency [28]. However, relatively low loading capacity of PS due to limited surface area of Au NPs and the possible early leakage of PSs during their circulation in biological systems have limited its therapeutic effects [29]. Mesoporous silica coated Au NPs (Au@mSiO_2) ensure high surface area [30] so that drug storage capacity can be improved significantly. Therefore the integration of mesoporous silica with Au NPs to form core-shell composite microspheres is undoubtedly of great interest for practical applications because it allows simultaneous chemo-photodynamic therapy in one system. Nevertheless, excess of cetyltrimethylammonium bromide (CTAB) surfactant as the common shape-directing agent was used to engineer GN which results in unwanted toxic for various clinical applications.

Herein, we reported a multimodal drug delivery system based on Au@mSiO_2, in which Au NPs acted as PDT-assistor cores and mesoporous silica shell templated by C_{18}TMS as supporters to load anticancer drugs. DOX and PS (Ce6) were expected to achieve

combined chemo-photodynamic therapy (Scheme 1). Moreover, Au NPs assisted to excite Ce6 effectively under the single continuous wave laser at 660 nm thus producing enhanced PDT. The mesoporous silica shell with less toxicity possessed facile surface modification as well as high drug loading capacity and controlled drug release. The efficient loading of Ce6 and DOX in Au NPs was evaluated and the uptake of nanoparticles by HeLa cells was traced as well. Compared with the treatment of DOX or Ce6 independently, the chemo-photodynamic combined treatments exhibited a more efficient cell inhibition in vitro.

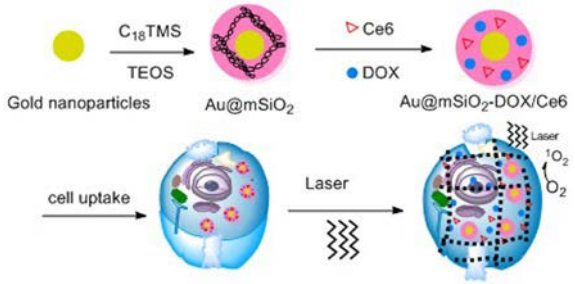

Scheme 1. Schematic illustration of $Au@mSiO_2$ nanocarrier preparation and application in combined chemo-photodynamic treatment against tumor cells

2. Experimental Section

2.1. Materials

Hydrogen tetrachloroaurate(III) trihydrate ($HAuCl_4 \cdot 3H_2O$, 99.999%), $C_{18}TMS$ (technical grade, 90%), tetraethyl orthosilicate(TEOS, 98%) and L-histidine (99%) was purchased from Sigma-Aldrich.-Caprolactone. Chlorin e6 (95%) was purchased from J&K Scientific. DOX·HCl and paclitaxel were purchased from Dalian Meilun Biology Technology Co., Ltd. N, N-dimethyl-4-nitrosoaniline (RNO, 98%) was purchased from Energy Chemical. Dulbecco's modified eagle medium (DMEM), fetal bovine serum (FBS), penicillin and streptomycin were all purchased from Invitrogen. HeLa cells were purchased from the KeyGEN Biotech and were cultured under the recommended conditions of 3-(4, 5-dimethyltlliazol-2-yl)-2, 5-diphenyltetrazoxium bromide (MTT) assay. All other chemicals used in this study were of analytical reagent grade and were used as received.

2.2 Preparation of Au NP

Au NPs were synthesized via a modified Frens method [31]. In a typical procedure, $HAuCl_4 \cdot 3H_2O$ (0.50 mM) aqueous solution was heated to boiling in a round bottom flask. Then, 800 uL of citrate solution (0.17 M) was added under vigorous stirring, and the mixture was kept on boiling for 30 min. Finally, Au colloid solution was centrifugated at 4000 rpm to remove the bulky grain. The supernatant was kept for further using.

2.3 Preparation of $Au@mSiO_2$ NPs

$Au@mSiO_2$ was prepared through the Stöber method [32]. 100 mL isopropanol and 15 mL Au colloid solution was mixed under vigorous stirring. Then ammonium hydroxide was added to adjust the pH to 10. After 10 min, different ratio of $C_{18}TMS$ / TEOS was added to form the silica shell on the Au NPs. After 24 h, the core-shell particles were precipitated by centrifugation at 8000 rpm for 3 min, and washed thoroughly with ethanol. The particles were finally dried and calcined in a tube furnace at 773 K for 5 h to acquire the mesoporous $Au@mSiO_2$ NPs.

2.4 Characterization

Transmission electron microscopy (TEM) was performed on a JEOL-2100 with accelerating voltage of 200 kV. TEM samples were prepared by drop-casting dispersion onto copper grids covered by carbon film. Ultrathin sections for Bio-TEM were cut with a diamond knife on a Leica ultracut R ultramicrotome. The X-ray powder diffraction patterns were recorded on a Bruker axs (D8 Advance) with CuK_α radiation. The surface area, pore size, and pore-size distribution of the samples were determined by Brunauer–Emmett–Teller(BET), nitrogen adsorption–desorption and Barrett–Joyner–Halenda (BJH) methods (BEL SORP-mini). Ultraviolet-visible spectra were collected using a LAMBDA-35 spectrometer. Confocal images were acquired using a Zeiss confocal laser scanning unit mounted on an LSM 710 fixed-stage upright microscope. The laser beam (660nm, 100 mW/cm^2) was purchased from Changchun New Industries Optoelectronics Technology Co., Ltd.

2.5 Drug loading

For DOX loading, $Au@mSiO_2$ (30 mg dispersed in 30 mL PBS) and DOX solutions (30 mg dispersed in 30 mL PBS) were stirred at room temperature for 2 days to reach the equilibrium state [33]. The DOX-loaded $Au@mSiO_2$ was collected by centrifugation at 10, 000

rpm for 10 min and was washed with water to remove the physically adsorbed DOX. The amount of loaded drug for Au@mSiO$_2$ was determined by a UV-Vis spectrophotometer at 480 nm. [34, 35]. The Ce6 loading experiment was conducted by the same protocol, except that Ce6 was determined at 404 nm. Loading of both Ce6 and DOX into the Au@mSiO$_2$ NPs was performed by adding Ce6 solutions (30 mg dispersed in 30 mL PBS) to Au@mSiO$_2$ (30 mg dispersed in 30 mL PBS) and stirring for 24 h, followed by the addition of DOX (30 mg dispersed in 30 mL PBS). Next, the mixture was stirred for another 24 h. For workup, the unbound Ce6 and DOX were removed by filtration through a 100-kDa filter (Millipore) and drug-loaded Au@mSiO$_2$ NPs were centrifuged at 8000 rpm. Then drug-loaded Au@mSiO$_2$ NPs were washed with water to remove the physically adsorbed DOX and Ce6. The loading ratio of Ce6 and DOX was measured by the absorbance at 404 and 480 nm, respectively. [36]

2.6 In vitro measurement of singlet oxygen generation

The generation of singlet oxygen from Ce6 was determined following the previous reports [37, 38]. RNO was used as a single oxygen sensor. Free Ce6 (100 mg mL^{-1}) and Ce6-loaded Au@mSiO$_2$ (100 mg mL^{-1} of Ce6) dispersed in 1% DMSO aqueous solution were added to 1 ml 1% DMSO aqueous solution containing 300 uL of L-histidine and 100 uL RNO (250 uM). Then, each solution was located in 1 mL quartz cuvette and irradiated by 660 nm laser at the light power density of 100 mW/cm^2 for different periods of time. The generation of singlet oxygen by Ce6 or Ce6-loaded Au@mSiO$_2$ would result in the bleaching of RNO absorption at 440 nm as a function of time thus reflects the production of $^1O_2$.

2.7 Cell culture and uptake

HeLa cell lines were maintained in Dulbecco's modified Eagles Medium (DMEM) containing 10% fetal bovine serum, 100 units mL^{-1} penicillin, and 100 mg mL^{-1} streptomyc in 37 ℃, 5% CO_2. In order to investigate the targeting property of drug-loaded Au@mSiO$_2$, 4',6-diamidino-2-phenylindole (DAPI) was used to locate the nucleus. In a typical procedure, 2.5 × 10^4 cells were seeded in a 35-mm dish with glass bottom for 24 h to allow the cells to attach. After the cells were washed twice with PBS, non-drug loaded Au@mSiO$_2$ NPs, drug loaded Au@mSiO$_2$ NPs were added to the dishes in a concentration of 20 μg mL^{-1}. After 4 h incubation, the cells were washed several times with PBS to remove the remaining samples and dead cells. Finally, the cells were observed under a confocal laser scanning microscope (CLSM, Carl Zeiss LSM 710) to trace their cell uptake.

2.8 Bio-TEM observations for HeLa cells

The HeLa cells were incubated with 100 μg mL^{-1} Au@mSiO$_2$ NPs in DMEM medium in 5% CO_2 at 37°C for 24 h. Afterwards, cells were washed three times with PBS and subsequently fixed with 2.5% glutaraldehyde in 0.03 M potassium phosphate buffer for at least 24 h. Cells were then washed with PBS, postfixed with 1% osmium tetroxide in sodium carboxylate buffer, washed with 0.05 mol L^{-1} maleate, and stained with 0.5% uranylacetate (Sigma Aldrich) in maleate buffer. After washing the cells in 0.05 mol L^{-1} maleate, the cells were dehydrated in a grading series of ethanol followed by acetone, embedded in Epon, and dried in an oven at 60 ℃ for 4 days. Ultrathin sections of approximately 50 nm thick were cut with a diamond knife on a Leica ultracut R ultramicrotome and transferred to the copper grid. The images were viewed on JEOL-2100 electron microscopy.

2.9 Photodynamic treatment and cell viability assay

The cytotoxicity in vitro was measured by using the MTT assay aginst HeLa cells. In a typical procedure, cells were initially seeded into a 96-well cell culture plate at 1×10^4 per well and then incubated for 24 h at 37 ℃ under 5% CO_2. DMEM solutions of non-drug loaded Au@mSiO$_2$ NPs and drug-loaded Au@mSiO$_2$ NPs at different concentrations were added under the same condition. After incubation for 24 h, cells were irradiated by the 660 nm laser) at a power density of 100 mW/cm^2 for 10 min [39, 40]. (The laser beam covered the whole well). The cells were further incubated for 48 h at 37 ℃ under 5% CO_2. The cells were washed three times with 0.2 mL PBS to remove the unbound NPs. Subsequently, 0.2 mL DMEM and 25 μL MTT (5 mg mL^{-1}) were added to each well and incubated for an additional 4 h at 37°C under 5% CO_2. Then the medium solution was replaced by 0.15 mL DMSO solution. After 10 min, the optical density at 490 nm (absorption value) of each well was measured on a Luminometer. Paclitaxel was used to be positive control.

Results and Discussion

The core-shell structured Au@mSiO$_2$ NPs were synthesized via a facile method of direct hydration and condensation of tetraethoxysilane (TEOS) and C_{18}TMS on the surface of citrate capped Au NPs [23] (Scheme 1). The TEM image in Figure 1a shows that the diameter of the Au NPs is around 20 nm and Au NPs possess high dispersability. Compared with the merely TEOS condensation(Figure 1b), the introdution of C_{18}TMS with a long alkyl chain accompanied TEOS, produces sparse silica polymerization, and gives rise to pores inside the silica networks after calcination at 773 K for 5 h in air (Figure 1c). The high-resolution TEM in Figure 1c (inset) further reveals that a crystalline lattice fringe of 0.237 nm is corresponding to the reflection of (111) lattice of Au NPs [41]. Moreover, the surface of the silica shell becomes rougher as the molar ratio of C_{18}TMS increased (Figure 1d-f), for C_{18}TMS causing the sparse and irregular polymerization of the silica networks.

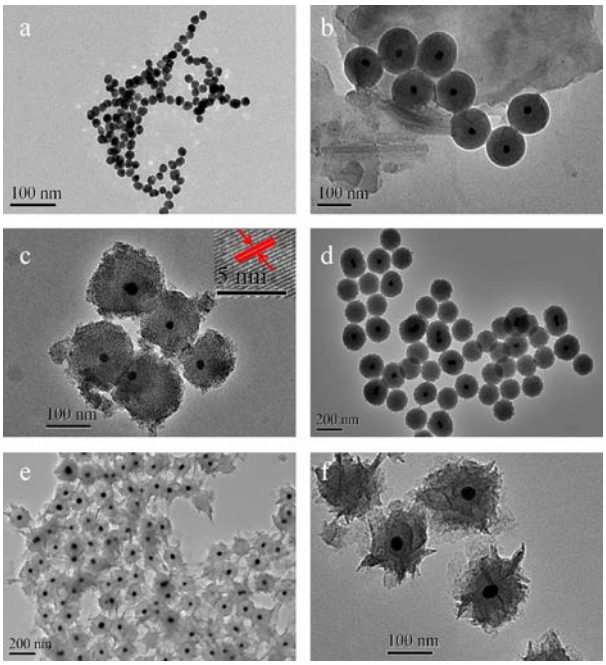

Figure 1. TEM images of (a) Au NPs, (b) Au@SiO_2, (c)Au@mSiO_2 after calcinations, inset: High-resolution TEM image of the crystalline lattice fringes of the Au NPs, (d)- (f) Au@mSiO_2 with the concentration ratios of C_{18}TMS and TEOS being 0.06, 0.08 and 0.10 respectively

X-ray diffraction (XRD) was used to identify the crystal phases of the Au@mSiO_2 NPs. As seen from Figure 2a, a wide and weak peak located at 2 θ = 22 ° can be assigned to the amorphous silica coating [42]. Apart from the peak of SiO_2, all of the patterns agree with the standard card of Au NPs.

Furthermore, the nitrogen (N_2) adsorption–desorption isotherm demonstrate the mesoporous structure characteristics of Au@mSiO_2 NPs (Figure 2b). The pore size distribution (Figure 2, inset) exhibits a sharp peak centered at a mean value of 3.7 nm. The BET surface area and total pore volume of the core–shell NPs were measured to be 137 m^2 g^{-1} and 0.4954 cm^3 g^{-1} respectively [35, 43, 44]. C_{18}TMS with a long alkyl chain accompanied TEOS can be deposited to form the silica shell network and gave rise to disordered pores inside the silica networks after calcinations. As the ratio of C_{18}TMS increased, the surface area and pore volume will be improved. Thus, the ideal mesoporous core-shell structure was constructed to be a candidate nanocarrier for its high drug loading property.

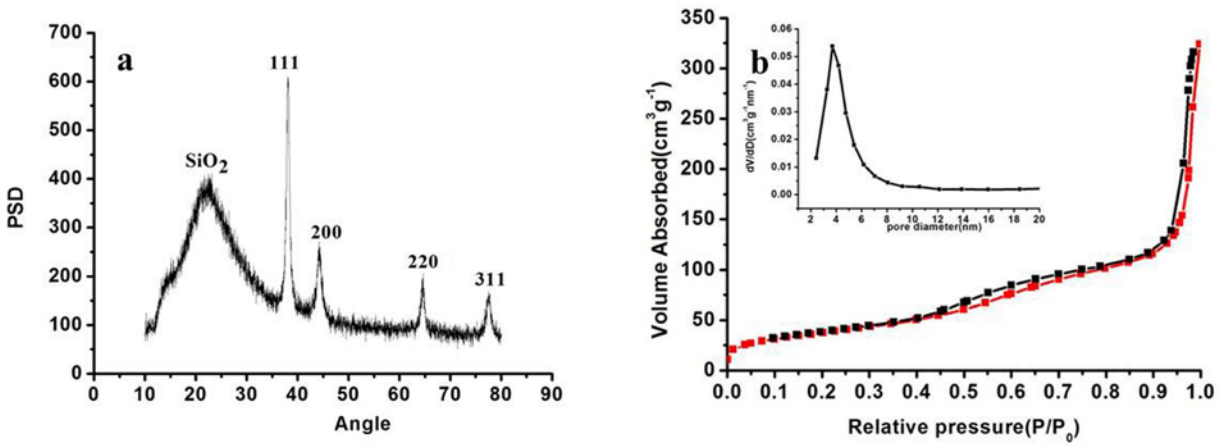

Figure 2. (a) XRD pattern of as-synthesized Au@mSiO_2, (b) N_2 adsorption–desorption isotherms and pore size distribution (inset) of as-synthesized Au@mSiO_2 NPs. [C_{18}TMS]/[TEOS]=0.1

DOX and Ce6, represented as two anticancer therapeutic agents with different mechanisms, were loaded into the mesoporous surface of Au@mSiO_2 NPs. The UV–vis absorbance evidenced that 12 mg of DOX could be immobilized per 30 mg Au@mSiO_2, while 24 mg Ce6 could be immobilized per 30 mg Au@mSiO_2. The fluorescence efficiency of Ce6 is the key factor in photodynamic therapy. In order to study the influence of the silica coating, we compared the fluorescence of Ce6 and Au@mSiO_2-Ce6 based on the excitation wavelength of Ce6 at 404 nm. In contrast to the free Ce6, the fluorescence of Ce6 inside the Au@mSiO_2 wasn't quenched (Figure 3a), which implied that the photosensitive capacity of Ce6 remained after it was loaded with the silica shell. So we deduced that Ce6 was absorbed through the mesoprous structure of Au@mSiO_2 which is more suitable for PDT.

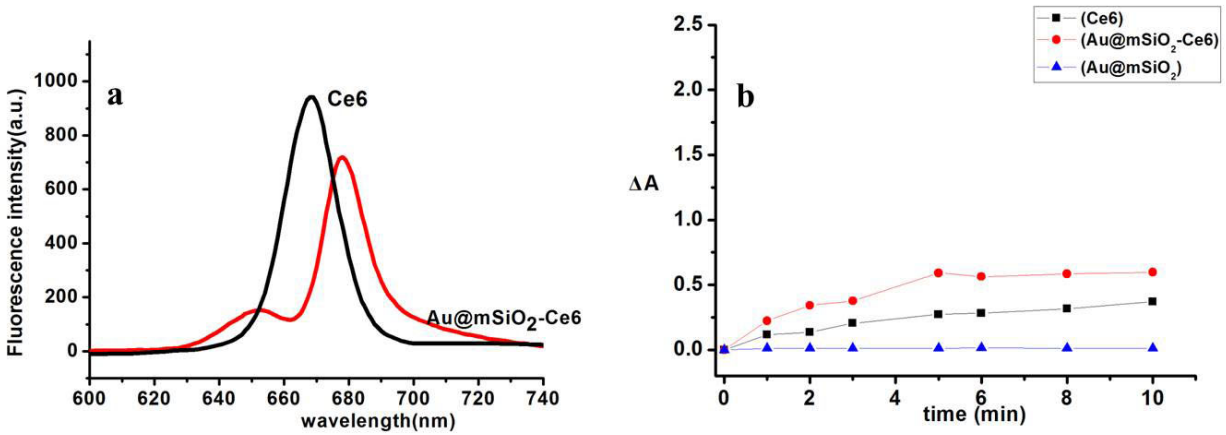

Figure 3. (a) Fluorescence spectra of Ce6 and Au@mSiO$_2$-Ce6 (Au@mSiO$_2$ ([C_{18}TMS]/[TEOS]=0.1), (b) Time-dependent bleaching of RNO caused by the singlet oxygen generation from free Ce6, Au@mSiO$_2$ and Au@mSiO$_2$-Ce6 at 660 nm irradiation

It should be emphasized that the ability of singlet oxygen generation was the critical criteria to assess the effect of PDT. Since singlet oxygen is difficult to be detected for its short lifetime, we detected the generation of $^1O_2$ by the bleaching of RNO [29-30]. As shown in Figure 3(b), the decrease in absorbance of RNO on account of Au@mSiO$_2$-Ce6 behaved as a function of time (Figure 3b), which indicated that the ability of Ce6 to develop $^1O_2$ remains after silica coating layer compared to free Ce6. Specially, by comparison, the quenching effect of $^1O_2$ production from Ce6 inside Au@mSiO$_2$ appears to be more drastic owing to the presence of Au NPs, which is in coincidence with the related report. However, Au@mSiO$_2$ alone cannot generate $^1O_2$. As the previous report, the proximity of Ce6 to the core of Au@mSiO$_2$ NPs is necessary thus enable efficient energy transmitted from Au NPs to Ce6. As a result, Au NPs would enhance the efficacy of $^1O_2$ caused by Ce6 for killing cancer cells.

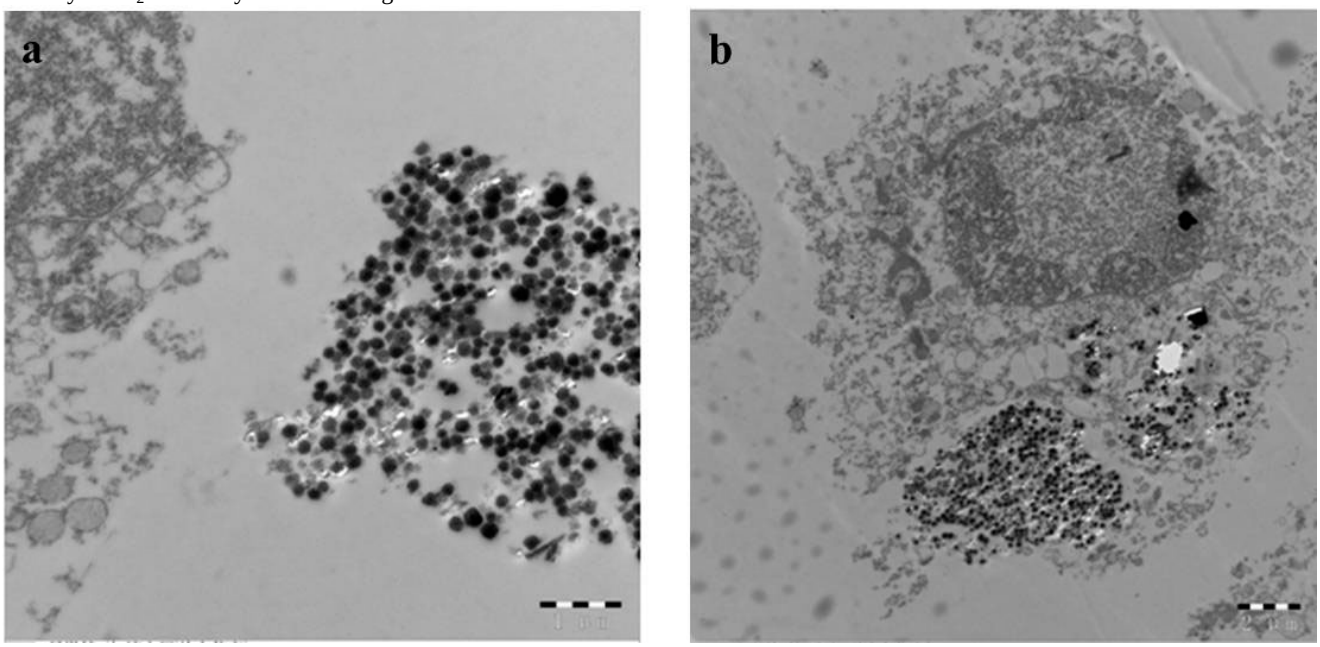

Figure 4. Bio-TEM images of HeLa cells after 24 h exposure to NPs (20 μg mL^{-1}).

With regard to a successful drug delivery system, one desirable property is that it can increase cell uptake ability and can be accumulated in the tumor cells to acquire the ideal therapy and decrease the side effects as far as possible [33]. Bio-TEM is a common characterization approach to validate the cellular uptake directly [45-47]. Consequently, we detected the internalization of Au@mSiO$_2$–DOX/Ce6 by HeLa cells using Bio-TEM. As shown in Figure 4a, the nanoparticles gathered outside of the cell membrane. Afterwards, they were distributed in the cytoplasm without entering the cell nucleus (Figure 4b). Additionally, some aggregates of these drug carriers were clearly observed as black patches inside the cell cytoplasm. The results of the Bio-TEM offer firm evidence that Au@mSiO$_2$ as the drug nanocarrier can be effectively uptaken by the cell via endocytosis process. Combing the Bio-TEM with the further CLSM results, the nanocarriers were testified to transport drugs into the tumor by the endocytosis and then accumulated into the cytoplasm for cancer

therapy.

This possible mechanism was confirmed by confocal microscopy results. As the experiment, the culture dishes were firstly incubated with Au@mSiO$_2$-DOX/Ce6 (20 μg mL $^{-1}$) and non-drug loaded Au@mSiO$_2$ NPs (20 μg mL $^{-1}$) for 4 h and were then irradiated by different excitation wavelengths to achieve the excitation and irradiation. The blue regions for cell nucleus dye DAPI, yellow regions for DOX, and red regions for Ce6 were used to monitor the target ability of drug carriers [33]. DAPI as a popular nuclear dye was used to locate the nucleus in the experiment. As the yellow region demonstrates, DOX was released into the nucleus delivered by Au@mSiO$_2$ so that it may perform chemotherapy through inhibiting DNA and RNA replication and transcription [48]. It is noted that the Ce6 is also entering the cells as the red region proved. It allows the generation of $^1O_2$ in the cell to achieve PDT based on the 660 nm laser to result in the final cell. In comparison, the fluorescence signals of non-drug loaded Au@mSiO$_2$ NPs based on the relative wavelength were much weaker when HeLa cells were incubated with drug-loaded Au@mSiO$_2$ NPs for 4h [49] . Hence, CLSM images detected that after cell uptake the drugs loaded in the mesoporous shell of Au@mSiO$_2$ were supposed to be subsequently accumulated in the cells and may perform possible anti-tumor effect.

Although mesoporous materials have been reported to be appropriate for drug delivery [50], it is necessary to investigate the cytotoxicity of Au@mSiO$_2$ under the laser exposure by MTT assays. Au@mSiO$_2$ without the laser exposure was carried out as control. The results showed that Au@mSiO$_2$ with the 660 nm laser exposure possess similar low cytotoxicity and only a relatively tumor cell death rate was observed even at a high concentration of 0.1 mg mL^{-1} compared to that without laser exposure (Figure 6a). It means that the Au@mSiO$_2$ nanoparticle itself owns non-toxicity and can be used as a safe drug carrier at a proper concentration even exposed to the laser.

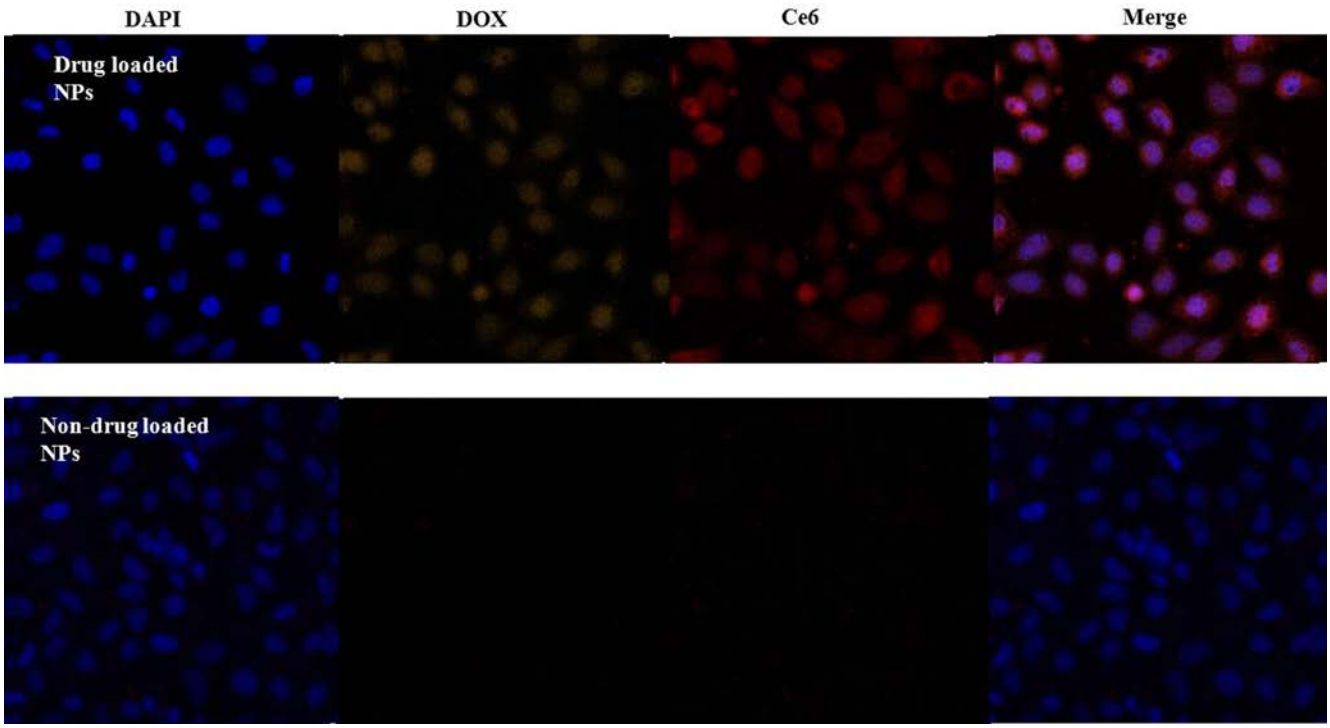

Figure 5. Confocal laser scanning microscope images of subcellular localization of Au@mSiO$_2$-DOX/Ce6 and non-drug loaded Au@mSiO$_2$ after 4h incubation with HeLa cells. The excitation wavelengths of DAPI stained (blue), DOX (yellow) Ce6 (red) are 360 nm, 488 nm and 633 nm respectively

As demonstrated in previous reports, the high hydrophobicity hinders free Ce6 from crossing the cell membrane to perform PDT effect in tumor cells even under laser irradiation. As for DOX, the lack of targeting leads to the server side effects. While Au@mSiO$_2$ nanocarrier may delivery more drug molecules into the tumor cells through endocytosis mediated to overcome the above shortcoming, which was demonstrated by the cell viability assay in vitro. In Figure 6b, we found that DOX-loaded Au@mSiO$_2$ showed a similar slight enhanced cell inhibition as Au@mSiO$_2$ after laser irradiation for the reason that DOX releasing wasn't affected by the laser. However, Figure 6c reflected that Au@mSiO$_2$-Ce6 possessed a considerably low inhibition before the laser exposure (Table 1). After that, Au@mSiO$_2$-Ce6 exhibited significantly increased cell inhibition. Therefore we conclude that PDT is an effective approach aiming at tumor treatment and can be achieved only when the laser is employed. In order to evaluate the synergistic chemotherapy and PDT effect, DOX and Ce6 was co-loaded into the Au@mSiO$_2$. It was not surprising that the IC_{50} of the Au@mSiO$_2$-DOX/Ce6 is higher than that of Au@mSiO$_2$-DOX in lack of laser irradiation (Table 1), since the loading efficacy of DOX was relatively lower when DOX and Ce6 were simultaneously loaded in the shell of Au@mSiO$_2$. However, after irradiation, Au@mSiO$_2$-DOX/Ce6 shows the higher tumor cells

inhibition than that of Au@mSiO$_2$-DOX and that of Au@mSiO$_2$-Ce6. The charming effects prove that laser-triggered PDT effect of Au@mSiO$_2$-DOX/Ce6 was executed in comparison upon 660 nm laser along with the chemotherapy. Au@mSiO$_2$-DOX/Ce6 unified two therapeutic modes into the single nanocarrier: chemotherapy through DOX and PDT through Ce6 which generates $^1O_2$ to kill tumor cells cooperatively. Such encouraging combination of chemotherapy and PDT into a platform can significantly enhance the curative effect compared to traditional monotherapy and therefore be expected to extend their applications in the biomedical field.

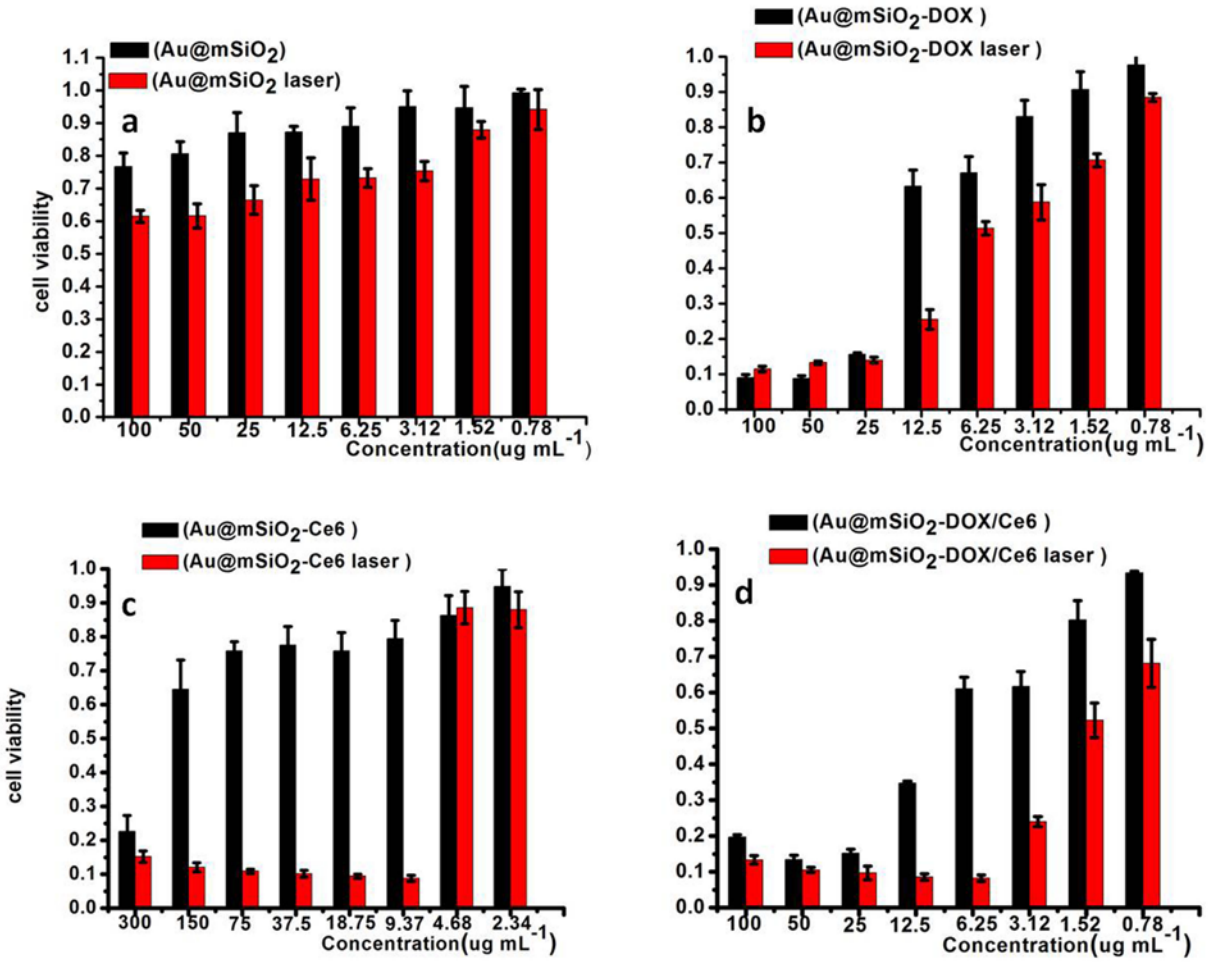

Figure 6. Cell viability data of HeLa cells incubated with (a) Au@mSiO$_2$, (b)Au@mSiO$_2$-DOX, (c) Au@mSiO$_2$-Ce6 and (d) Au@mSiO$_2$-DOX/Ce6, blank: without laser, red: with laser

Table 1. IC_{50} values (ug mL^{-1}) of the different NPs:

IC_{50}	Au@mSiO$_2$	Au@mSiO$_2$-DOX	Au@mSiO$_2$-Ce6	Au@mSiO$_2$- DOX /Ce6
Before laser	-	5.094	130.0	15.21
After laser	-	3.215	7.232	1.152

Conclusions

In this study, we undertook Au@mSiO$_2$ as a multimodal nanocarrier to load both DOX and Ce6 for combined chemo-photodynamic therapy. Introduction of C_{18}TMS can significantly produce mesoporous shell to achieve high drug loading efficiency. Moreover, the porous structure acts as a channel to enable Ce6 inside to generate $^1O_2$. Cytotoxicity assays demonstrated the low toxicity of Au@mSiO$_2$, which indicates that it can be regarded as a suitable safe drug carrier. More importantly, the results of CLSM and Bio-TEM evaluated that Au@mSiO$_2$ can significantly improve the uptake of DOX and Ce6 by tumor cells via endocytosis. As a consequence, more drug molecules can be delivered and accumulated in the tumor cells. Au@mSiO$_2$-DOX/Ce6 displays a better cell viability assay due to the collaboration of chemotherapy and PDT strategies into one platform, which will provide a new and encouraging way in the development of versatile cancer therapy for further applications.

Acknowledgement

We gratefully acknowledge Laboratory of Nano-chemistry in Nanjing University of the generous assistance to the part of the work. This study was also sponsored by the National Natural Science Foundation of China (No. 21401216) and the Fundamental Research Funds for the Central Universities. This work was also supported by Qing Lan Project in Jiangsu Province.

Notes and references

[a] *School of Sciences, State Key Laboratory of Natural Medicines, China Pharmaceutical University, Nanjing 211198, China.*
[b] *Key Laboratory of Biomedical Functional Materials, China Pharmaceutical University, Nanjing 211198, China.*
E-mail: zwy_1115@126.com

1. S. L. Zhang, Z. Q. Chu, C. Yin, C. Y. Zhang, G. Lin and Q. Li, *J Am Chem Soc*, 2013, **135**, 5709-5716.
2. Y. Wang, C. Zhang, H. M. Li, G. X. Zhu, S. S. Bao, S. Q. Wei, L. M. Zheng, M. Ren and Z. Xu, *J Mater Chem B*, 2015, **3**, 296-305.
3. A. K. Iyer, Z. F. Duan and M. M. Amiji, *Mol Pharmaceut*, 2014, **11**, 2511-2526.
4. S. R. MacEwan and A. Chilkoti, *Nano Lett*, 2014, **14**, 2058-2064.
5. H. M. Li, Z. Li, J. Zhao, B. Q. Tang, Y. H. Chen, Y. K. Hu, Z. D. He and Y. Wang, *Nanoscale Res Lett*, 2014, **9**.
6. R. C. Lv, P. P. Yang, F. He, S. L. Gai, C. X. Li, Y. L. Dai, G. X. Yang and J. Lin, *Acs Nano*, 2015, **9**, 1630-1647.
7. W. Wang, D. Xu, X. J. Wei and K. Z. Chen, *Int J Nanomed*, 2014, **9**, 4879-4891.
8. C. B. He, D. M. Liu and W. B. Lin, *Acs Nano*, 2015, **9**, 991-1003.
9. C. Wang, L. Cheng, Y. M. Liu, X. J. Wang, X. X. Ma, Z. Y. Deng, Y. G. Li and Z. Liu, *Advanced Functional Materials*, 2013, **23**, 3077-3086.
10. D. E. Dolmans, D. Fukumura and R. K. Jain, *Nat Rev Cancer*, 2003, **3**, 380-387.
11. R. Bonnett, *Chemical Society Reviews*, 1995, **24**, 19-33.
12. M. Price, L. Heilbrun and D. Kessel, *Photochemistry And Photobiology*, 2013, **89**, 683-686.
13. P. Zhang, W. Steelant, M. Kumar and M. Scholfield, *J Am Chem Soc*, 2007, **129**, 4526-+.
14. S. S. Cui, D. Y. Yin, Y. Q. Chen, Y. F. Di, H. Y. Chen, Y. X. Ma, S. Achilefu and Y. Q. Gu, *Acs Nano*, 2013, **7**, 676-688.
15. H. Park and K. Na, *Biomaterials*, 2013, **34**, 6992-7000.
16. A. E. O'Connor, W. M. Gallagher and A. T. Byrne, *Photochemistry And Photobiology*, 2009, **85**, 1053-1074.
17. H. R. Xiao, B. S. Zhu, D. L. Wang, Y. Pang, L. He, X. F. Ma, R. B. Wang, C. Y. Jin, Y. Chen and X. Y. Zhu, *Carbon*, 2012, **50**, 1681-1689.
18. J. Wang, G. Z. Zhu, M. X. You, E. Q. Song, M. I. Shukoor, K. J. Zhang, M. B. Altman, Y. Chen, Z. Zhu, C. Z. Huang and W. H. Tan, *Acs Nano*, 2012, **6**, 5070-5077.
19. B. Tian, C. Wang, S. Zhang, L. Z. Feng and Z. Liu, *Acs Nano*, 2011, **5**, 7000-7009.
20. H. Park, W. Park and K. Na, *Biomaterials*, 2014, **35**, 7963-7969.
21. Z. W. Li, C. Wang, L. Cheng, H. Gong, S. N. Yin, Q. F. Gong, Y. G. Li and Z. Liu, *Biomaterials*, 2013, **34**, 9160-9170.
22. B. S. Wong, S. L. Yoong, A. Jagusiak, T. Panczyk, H. K. Ho, W. H. Ang and G. Pastorin, *Advanced Drug Delivery Reviews*, 2013, **65**, 1964-2015.
23. J. Wang, M. X. You, G. Z. Zhu, M. I. Shukoor, Z. Chen, Z. L. Zhao, M. B. Altman, Q. Yuan, Z. Zhu, Y. Chen, C. Z. Huang and W. H. Tan, *Small*, 2013, **9**, 3678-3684.
24. L. Zhou, W. Wang, J. Tang, J. H. Zhou, H. J. Jiang and J. Shen, *Chemistry-a European Journal*, 2011, **17**, 12084-12091.
25. J. Gil-Tomas, L. Dekker, N. Narband, I. P. Parkin, S. P. Nair, C. Street and M. Wilson, *Journal Of Materials Chemistry*, 2011, **21**, 4189-4196.
26. K. Y. Huang, H. L. Ma, J. Liu, S. D. Huo, A. Kumar, T. Wei, X. Zhang, S. B. Jin, Y. L. Gan, P. C. Wang, S. T. He, X. N. Zhang and X. J. Liang, *Acs Nano*, 2012, **6**, 4483-4493.
27. P. Huang, J. Lin, W. W. Li, P. F. Rong, Z. Wang, S. J. Wang, X. P. Wang, X. L. Sun, M. Aronova, G. Niu, R. D. Leapman, Z. H. Nie and X. Y. Chen, *Angewandte Chemie-International Edition*, 2013, **52**, 13958-13964.
28. C. E. Chen, L. Zhou, J. Geng, J. S. Ren and X. G. Qu, *Small*, 2013, **9**, 2793-2800.
29. I. Gorelikov and N. Matsuura, *Nano Lett*, 2008, **8**, 369-373.
30. M. K. K. Oo, Y. M. Yang, Y. Hu, M. Gomez, H. Du and H. J. Wang, *Acs Nano*, 2012, **6**, 1939-1947.
31. X. H. Ji, X. N. Song, J. Li, Y. B. Bai, W. S. Yang and X. G. Peng, *J Am Chem Soc*, 2007, **129**, 13939-13948.
32. J. Lee, J. C. Park, J. U. Bang and H. Song, *Chemistry Of Materials*, 2008, **20**, 5839-5844.
33. H. Gong, L. Cheng, J. Xiang, H. Xu, L. Z. Feng, X. Z. Shi and Z. Liu, *Advanced Functional Materials*, 2013, **23**, 6059-6067.
34. X. J. Liu, Q. Wang, C. Li, R. J. Zou, B. Li, G. S. Song, K. B. Xu, Y. Zheng and J. Q. Hu, *Nanoscale*, 2014, **6**, 4361-4370.
35. C. Y. Yang, W. Guo, L. R. Cui, N. An, T. Zhang, H. M. Lin and F. Y. Qu, *Langmuir*, 2014, **30**, 9819-9827.
36. L. M. Zhang, J. G. Xia, Q. H. Zhao, L. W. Liu and Z. J. Zhang, *Small*, 2010, **6**, 537-544.
37. H. Y. Yoon, H. Koo, K. Y. Choi, S. J. Lee, K. Kim, I. C. Kwon, J. F. Leary, K. Park, S. H. Yuk, J. H. Park and K. Choi, *Biomaterials*, 2012, **33**, 3980-3989.
38. H. Koo, H. Lee, S. Lee, K. H. Min, M. S. Kim, D. S. Lee, Y. Choi, I. C. Kwon, K. Kim and S. Y. Jeong, *Chemical Communications*, 2010, **46**, 5668-5670.
39. P. Huang, J. Lin, X. S. Wang, Z. Wang, C. L. Zhang, M. He, K. Wang, F. Chen, Z. M. Li, G. X. Shen, D. X. Cui and X. Y. Chen, *Advanced Materials*, 2012, **24**, 5104-5110.
40. S. J. Wang, P. Huang, L. M. Nie, R. J. Xing, D. B. Liu, Z. Wang, J. Lin, S. H. Chen, G. Niu, G. M. Lu and X. Y. Chen, *Advanced Materials*, 2013, **25**, 3055-3061.
41. Z. L. Jiang, B. Dong, B. T. Chen, J. Wang, L. Xu, S. Zhang and H. W. Song, *Small*, 2013, **9**, 604-612.
42. W. Wei, Q. Zhang and X. W. Zheng, *Acta Chimica Sinica*, 2013, **71**, 387-391.
43. S. Kumar, A. Daverey, N. K. Sahu and D. Bahadur, *J Mater Chem B*, 2013, **1**, 3652-3660.
44. X. J. Kang, Z. Y. Cheng, C. X. Li, D. M. Yang, M. M. Shang, P. A. Ma, G. G. Li, N. A. Liu and J. Lin, *Journal Of Physical Chemistry C*, 2011, **115**, 15801-15811.
45. S. D. Huo, S. B. Jin, X. W. Ma, X. D. Xue, K. N. Yang, A. Kumar, P. C. Wang, J. C. Zhang, Z. B. Hu and X. J. Liang, *Acs Nano*, 2014, **8**, 5852-5862.
46. X. Ma, S. Sreejith and Y. L. Zhao, *Acs Applied Materials & Interfaces*, 2013, **5**, 12860-12868.

47. X. Y. Li, Q. J. He and J. L. Shi, *Acs Nano*, 2014, **8**, 1309-1320.

48. H. C. Yeh, C. M. Puleo, T. C. Lim, Y. P. Ho, P. E. Giza, R. C. C. Huang and T. H. Wang, *Nucleic Acids Research*, 2006, **34**.

49. P. Huang, J. Lin, S. J. Wang, Z. J. Zhou, Z. M. Li, Z. Wang, C. L. Zhang, X. Y. Yue, G. Niu, M. Yang, D. X. Cui and X. Y. Chen, *Biomaterials*, 2013, **34**, 4643-4654.

50. Y. P. Li, W. W. Xiao, K. Xiao, L. Berti, J. T. Luo, H. P. Tseng, G. Fung and K. S. Lam, *Angewandte Chemie-International Edition*, 2012, **51**, 2864-2869.